Theor Chim Acta (1995) 90: 357–381

Theoretica Chimica Acta

A two-dimensional model for collisional energy transfer in bimolecular ion–molecule dynamics: $M^+ + (H_2; D_2; \text{or HD}) \rightarrow (MH^+ + H; MD^+ + D; MH^+ + D; \text{or } MD^+ + H)$

Monique Revorêdo Chacon-Taylor, Jack Simons
Chemistry Department, University of Utah, Salt Lake City, UT 84112, USA

Received April 1, 1994/Final revision received August 2, 1994/Accepted August 29, 1994

Summary. Guided ion beam kinetic energy thresholds in the ion–molecule reactions $M^+ + H_2 \rightarrow MH^+ + H$, where M^+ is a closed-shell atomic ion B^+, Al^+, or Ga^+, were found to exceed by 0.4 to ca. 5 eV the thermodynamic energy requirements (or the theoretically computed barrier heights) for these reactions. In addition, the formation of MD^+ occurs at a significantly lower threshold than MH^+ when M^+ reacts with HD. Moreover, the measured reaction cross-sections for the production of MH^+ or MD^+ product ions are very small (10^{-17} to 10^{-20} cm^2), being largest for B^+ and smallest for Ga^+. A previous paper from this group proposed that collisional-to-internal energy transfer is the rate-limiting step for this class of reactions. It also suggested, based on a dynamical resonance picture, that collisions occurring at or near C_{2v} symmetry are more effective than other collisions even though C_{2v} geometries provide no lower potential energy barriers than others. By examining the collision paths characteristic of flux early in the bimolecular collision and searching for geometries along such paths where collisional-to-internal energy transfer is optimal, our earlier efforts predicted reaction thresholds in reasonable agreement with the (previously perplexing) experimental data. In the present work, we introduce a model Hamiltonian whose classical and quantum dynamics we apply to the $M^+ + H_2$, D_2, HD reactive collisions. We calculate the classical collisional-to-internal energy transfer cross-sections and find energy transfer thresholds that resemble the experimental reaction thresholds but whose isotopic mass trends are not entirely consistent with experiment. We then use a Green function method and a local quadratic approximation to the potential surface to obtain analytical expressions for the isotopic mass dependences of the collisional-to-vibrational energy transfer and for the subsequent fragmentation of the three-atom system. Finally, we analyze the origin of the threshold energy asymmetry in the $M^+ + HD$ reactions.

Key words: Collisional energy transfer – Bimolecular ion-molecule dynamics

1 Introduction

Guided ion beam measurements of the cross-sections [1] for the production of MH^+ and MD^+ product ions in reactions of closed shell ^1S B^+, Al^+, and Ga^+

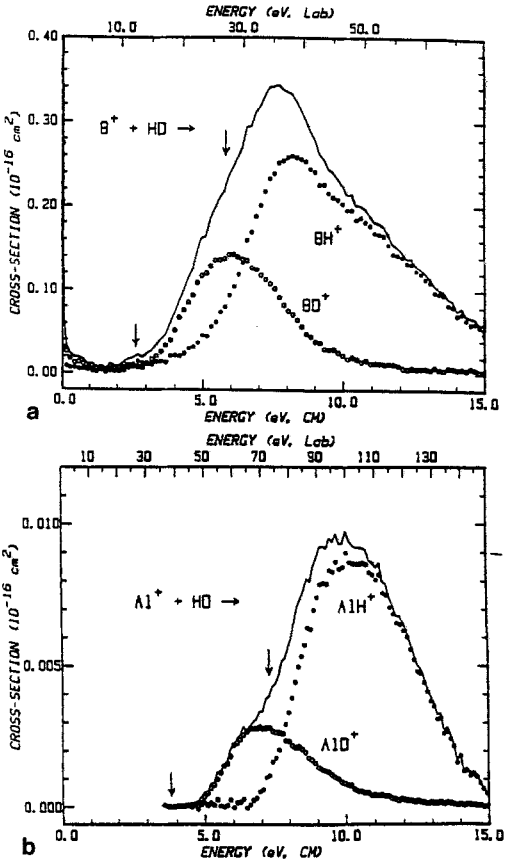

Fig. 1. Cross-sections for reactions for B^+ (^1S) (**a**) and Al^+ (^1S) (**b**) as a function of kinetic energy in the center-of-mass frame (lower scale) and laboratory frame (upper scale). Arrows indicate the thermodynamic thresholds for formation of the $X^2\Sigma^+$ and $A^2\Pi$ states of the products[1]

ions (denoted M^+) with closed-shell $^1\Sigma_g^+$ H_2, D_2 and HD displayed features that required further interpretation:

- The apparent thresholds (i.e., the collision kinetic energies where product MH^+ or MD^+ ions are first formed) exceed the minimum thermodynamic energy requirements by significant amounts (e.g., by up to 5 eV for Ga^+). Two examples of these data are shown in Fig. 1.
- In experiments with HD, MD^+ formation displays a lower energy threshold than MH^+ (see Fig. 1.)
- The cross-sections are small (10^{-17} to 10^{-20} cm^2), and are smallest for Ga^+ and largest for B^+.

Impulsive, statistical, and spectator–stripper models [2] do not succeed in rationalizing the unexpectedly high threshold energies or the magnitudes of the MD^+/MH^+ threshold energy asymmetries. For example, an impulsive model decomposes the collision kinetic energy T for the M^+HD case into components $T_{MH} \cong \frac{1}{3}T$ and $T_{MD} = \frac{2}{3}T$ that give the kinetic energy of M^+ relative to the H and D atoms, respectively. Such a model then predicts that MD^+ formation can occur at a lower total collision energy T because $\frac{2}{3}$ of this energy is available to the M–D coordinate. In particular, the model predicts that the threshold kinetic energy for MD^+ formation should be $(\frac{1}{3})/(\frac{2}{3}) = \frac{1}{2}$ that for MH^+ formation in the $M^+ + HD$

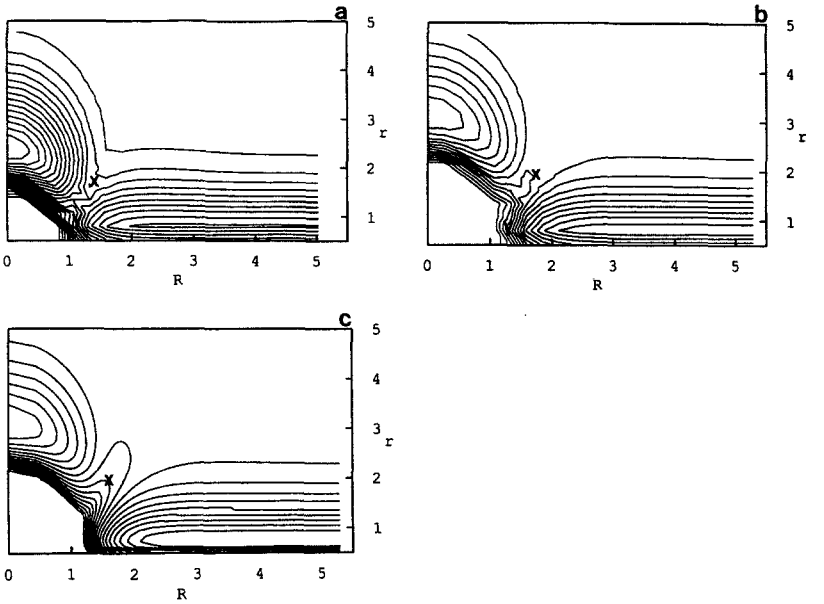

Fig. 2. **a** C_{2v} symmetry contour plot of the ($^1A_1$) ground state energy of $B^+ + H_2$. The R (the distance of B^+ to the center of H–H) and r (H–H distance) axes are in Ångstroms, and the contours are spaced by 10.0 kcal/mol. **b** C_{2v} symmetry contour plot of the ($^1A_1$) ground state energy of $Al^+ + H_2$. The R (the distance of Al^+ to the center of H–H) and r (H–H distance) axes are in Ångstroms, and the contours are spaced by 10.6 kcal/mol. **c** C_{2v} symmetry contour plot of the ($^1A_1$) ground state energy of $Ga^+ + H_2$. The R (distance of Ga^+ to the center of H–H) and r (H–H distance) axes are in Ångstroms, and the contours are spaced by 10.4 kcal/mol. In **a–c**, the symbol X is used to denote the location of the barrier, and Y is used to denote the region of strong mode mixing [3]

case; this quantitative prediction is not seen in the experimental data. In contrast, a previous work [3] by one of the authors and collaborators proposed that entrance-channel transfer of M^+–H_2 relative translational energy to H_2 vibrational energy is the rate-limiting step in this class of reactions.

By considering *collision paths* characteristic of early reactant flux, in which the H_2, D_2 or HD internuclear distance is essentially undisturbed from its equilibrium value (because the experiments involve room temperature hydrogen gas), and searching, along these paths, for geometries at which energy transfer is predicted by a resonance condition to be optimal, Ref. [3] made predictions of reaction thresholds reasonably in agreement with the experimental findings. It is the purpose of the present work to make more quantitative the energy-transfer rate-determining-step picture and to carry out classical simulations and quantal dynamical analyses on a model potential surface fit to the *ab initio* data of Ref. [3] to gain further insight into this class of reactions.

We approach the problem in the following manner:

1. We fit the same *ab initio* C_{2v} and near-C_{2v} potential energy surfaces employed in Ref. [3] (see Fig. 2) to extract strength and range parameters characteristic of the repulsive portion of the M^+–H_2 surface implicated in Ref. [3] as the regions near which dynamical resonances can occur. We use the undisturbed H–H potential to characterize the H_2, D_2, or HD vibration (because Ref. [3] showed the dynamical

resonances to occur at geometries where one of the local normal mode frequencies was nearly equal to that of the isolated hydrogenic molecule). And we use limited locally computed *ab initio* estimates of the coupling strength between the H–H and M^+–H_2 coordinates.
2. We employ the potentials created in step 1 to introduce a two-dimensional model Hamiltonian to describe the collisional energy transfer entrance-channel part of the reaction.
3. We use an adaptive-step-size fifth-order Runge–Kutta method [4] to propagate classical trajectories and obtain the cross-section for the T–V energy transfer. Trends in the T–V energy transfer onsets correlate with the experimental thresholds, and $v = 0 \rightarrow v = 1$ excitation is seen to dominate near the threshold. However, the isotopic mass effects displayed in the classical trajectory data are not entirely consistent with the experimental results (which suggests that there is more to the reaction cross-section than T–V energy transfer).
4. We also analyze the quantum transition probabilities for the T–V process using a Green function method, to further quantify the origin of the high energy threshold and to achieve analytical expressions for the threshold energies that more clearly display the isotopic masses and potential surface parameters.
5. Finally, we analyze energy transfer for the HD case, and offer an explanation for the origin of the asymmetry in the MD^+ and MH^+ thresholds.

In Section 2 we develop the model Hamiltonian and describe the results of classical trajectory simulations using it. In Section 3, we describe the quantum propagator approach and make connection with the mode resonance picture of Ref. [3]. We also use classical coupled-oscillator concepts to address the threshold energy asymmetry in the M^+ + HD cases. Section 4 contains an overview of our findings.

2. The model Hamiltonian and classical trajectories

2.1 The model potential

Based on the evidence detailed in Ref. [3], we assume that near-C_{2v} collision geometries, with the H_2 moiety near its equilibrium internuclear distance, are optimally effective at allowing T–V energy transfer to occur. Of course, collisions occur at many orientations and many impact parameters that must be averaged over to compute the cross-section. However we expect from the earlier work that near-C_{2v} geometries, which necessarily have small impact parameters, will dominate the T–V process because only near such geometries does dynamical resonance occur between the M^+–H_2 collisional and H–H vibrational modes. We therefore introduce two coordinates x and y to describe the BC + A collision as shown in Fig. 3.

The M^+ + H–H internal potentials energy U is thus assumed to be a function of these two coordinates and the following two-dimensional model Hamiltonian is introduced:

$$H = -\frac{\hbar}{2\tilde{m}}\frac{\partial^2}{\partial x^2} - \frac{\hbar}{2\mu}\frac{\partial^2}{\partial y^2} + U(x, y).$$

As explained in Sect. 1, we choose to express $U(x, y)$ in terms of a M^+–H_2 repulsion which we describe as $v\exp(-ax)$, the unperturbed H–H potential

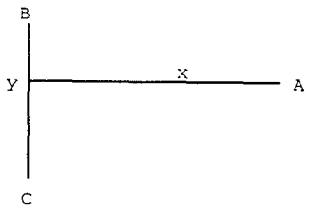

Fig. 3. Coordinates for near C_{2v} collisions (A denotes the M^+ ion and BC the H_2, D_2, or HD)

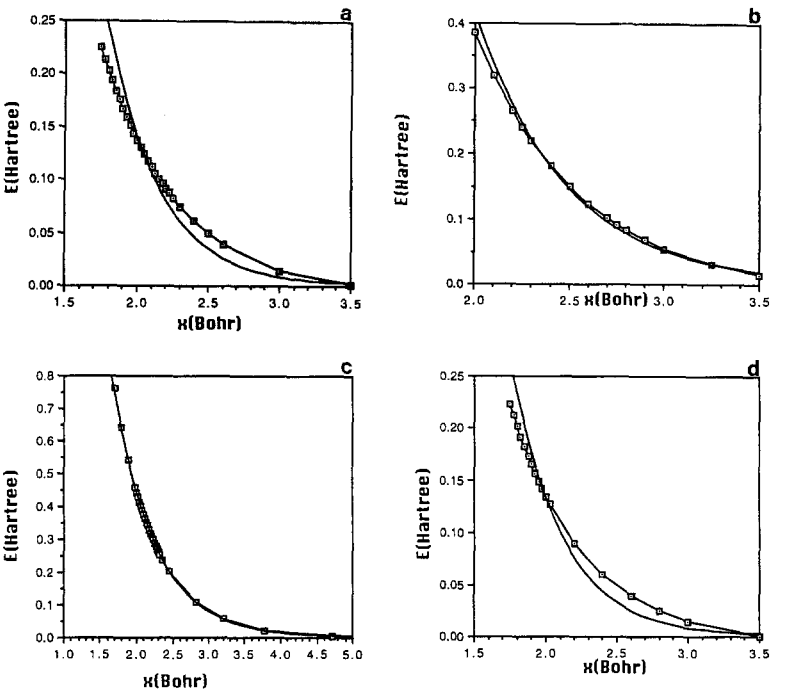

Fig. 4a. BH_2^+ surface fit, where $y = 1.405011$ a.u. $= 0.7435$ Å and 1.75 a.u. $< x <$ 3.5 a.u., $E = 39.173 \exp(-2.81145x)$; $R^2 = 0.936$; **b.** AlH_2^+ surface fit, where $y = 1.405011$ a.u. $- 0.7435$ Å and 2.0 a.u. $< x <$ 3.5 a.u., $y = 27.271 \exp(-2.091806x)$; $R^2 = 0.993$; **c** GaH_2^+ surface fit, $r_{H_2} = 1.405011$ a.u. $= 0.7435$ Å and 1.70 a.u. $< x < 4.7$ a.u., $E = 14.205 exp(-1.72899x)$; $R^2 = 0.999$; **d** BHD^+ surface fit where $y = 1.405011$ a.u. $= 0.7435$ Å and 1.75 a.u. $< x < 3.5$ a.u., $E = 37.182 \exp(-2.81399x)$; $R^2 = 0.933$

$\frac{1}{2} k_{BC}(y - y_{eq})^2$, plus a coupling which we embody in a b parameter computed as detailed below:

$$U(x, y) = v \exp(-ax - b(y - y_{eq})) + \tfrac{1}{2} k_{BC}(y - y_{eq})^2.$$

In this Hamiltonian, y is the distance between B and C, and x is the distance between A and the center of mass of BC.

The potential parameters a and v are obtained by fitting the *ab initio* computed data of Ref. [3] (plus additional data obtained by us) at several values of x, but with $y = y_{eq}$, to the $v \exp(-ax)$ functional form. Specifically, data in the narrow entrance channels of Fig. 2 ($r \approx 0.7$ Å, $R > 1.0$ Å) are used. Examples of such fits are shown in Fig. 4.

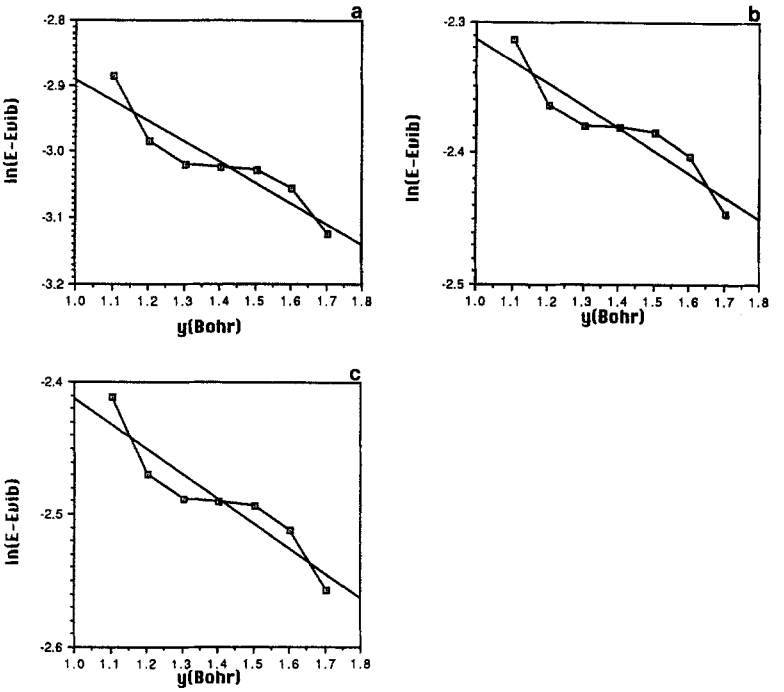

Fig. 5a. *Ab initio* (squares) and least-squares fit (solid line) energy for BH_2^+ as a function of vibrational coordinate y, $x = 2.50$ Bohr, $y^* = 1.460773$ Bohr, $k = 0.369333$ a.u., $E - E_{vib} = v \exp(-ax - b(y - y^*))$; $\ln(E - E_{vib}) = -2.5809 - 0.31132y$; $R^2 = 0.847$; **b** *Ab initio* (squares) and least-squares fit (solid line) energy for AlH_2^+ as a function of vibrational coordinate y, $x = 2.75$ Bohr, $y^* = 1.404289$ Bohr, $k = 0.369333$ a.u., $E - E_{vib} = v \exp(-ax - b(y - y^*))$; $\ln(E - E_{vib}) = -2.1422 - 0.17095y$; $R^2 = 0.861$; **c** *Ab initio* (squares) and least-squares fit (solid line) energy for GaH_2^+ as a function of vibrational coordinate y, $x = 3.00$ Bohr, $y^* = 1.414951$ Bohr, $k = 0.369333$ a.u., $E - E_{vib} = \exp(-ax - b^*(y - y^*))$; $\ln(E - E_{vib}) = -2.2229 - 0.18944y$; $R^2 = 0.859$

The b parameter describes the coupling between the collision (x) and vibrational (y) coordinates. Here, x_A is a representative value of x in the region where the model of Ref. [3] suggests energy transfer should occur (see Fig. 2), $U(x_A, y)$ is computed at several values of y (ranging ca. $\pm$ 0.4 Bohr from y_{eq}) in a fully *ab initio* manner. The quantity $\ln[U(x_A, y) - \frac{1}{2} k_{BC} (y - y_{eq})^2]$ is then plotted vs. y. According to our model potential, this logarithmic function should reduce to $\ln v - ax_A - b(y - y_{eq})$, so the slope of such a plot should give b. Examples of such plots are given in Fig. 5.

The values of v, a and b thus obtained and used for the reactions studied here are given in Table 1.

The appropriate effective masses appearing in the x and y kinetic energy expressions are

$$\tilde{m} = \frac{m_A(m_B + m_C)}{m_A + m_B + m_C}$$

and

$$\mu = \frac{m_B m_C}{m_B + m_C},$$

Table 1. The $v \exp(-ax - b(y - y_{eq}))$ portion of the $U(x, y)$ potentials used for different M^+, v is in Hartree, a and b are in $Bohr^{-1}$

B^+	$39.173 \exp(-2.81145x - 0.31132(y - y_{eq}))$
Al^+	$27.271 \exp(-2.09181x - 0.17095(y - y_{eq}))$
Ga^+	$14.205 \exp(-1.72899x - 0.18944(y - y_{eq}))$

Table 2. Values for the y-mode frequency and reduced mass μ

System	μ (a.u.)	ω_Y (a.u.)
H_2	918	0.0200 (0.54 eV)
HD	1224	0.0174 (0.47 eV)
D_2	1836	0.0142 (0.39 eV)

Table 3. Collisional mass $\tilde{m}$, and mass-weighted repulsion (Γ) and coupling (K) parameters

System	$\tilde{m}$ (a.u.)	Γ (a.u.)	$K^2 = \frac{\tilde{m}}{\mu}\frac{b}{a}$	$\frac{\hbar \Gamma^2 K^2}{\omega_Y}(10^{-3})$
BH_2^+	3107	0.0504	0.0415	5.3
BHD^+	4328	0.0427	0.0434	4.5
BD_2^+	5386	0.0383	0.0360	3.7
AlH_2^+	3419	0.0358	0.0249	1.6
AlHD	4958	0.0297	0.0270	1.4
AlD_2^+	6397	0.0261	0.0233	1.1
GaH_2^+	3570	0.0289	0.0467	1.9
$GaHD^+$	5282	0.0238	0.0518	1.7
GaD_2^+	6947	0.0207	0.0454	1.4

which, for the cases at hand, are listed in Tables 2 and 3. Notice that in the limit where $m_A \gg (m_B + m_C)$ (e.g., for Ga^+ but less so for B^+), $\tilde{m} \cong m_B + m_C$, so both μ and $\tilde{m}$ depend only on the masses of the B and C atoms, not on the mass of the metal ion.

2.2 Mass weighted coordinates

The above Hamiltonian can be rewritten in terms of mass-weighted coordinates $X = x\sqrt{\tilde{m}}$ and $Y = (y - y_{eq})\sqrt{\mu}$ as

$$H = -\frac{\hbar^2}{2}\frac{\partial^2}{\partial X^2} - \frac{\hbar^2}{2}\frac{\partial^2}{\partial Y^2} + V(X, Y) + \tfrac{1}{2}\omega_Y Y^2,$$

where $V(X, Y) = v \exp(-\Gamma(X - KY))$,

$$\Gamma = \frac{a}{\sqrt{\tilde{m}}}$$

and

$$K = \frac{-b}{a}\sqrt{\frac{\tilde{m}}{\mu}} \quad \left(\text{so } \Gamma \mathbf{K} = \frac{-b}{\sqrt{\mu}}\right)$$

are the mass-weighted versions of the range (a) and coupling (b) parameters, and

$$\omega_Y^2 = \frac{k_{BC}}{\mu}$$

is the square of the Y-mode harmonic frequency.

For the ion–molecule collisions under study here, the values of v, Γ^2, K^2, $\Gamma^2 K^2$, and ω_Y are given in Tables 1–3.

The mass-weighted coordinates are introduced here and used in subsequent classical and quantal calculations because the findings of Ref. [3] cause us to emphasize the *local frequencies* of motion along x and y in anticipation of the dynamical resonances postulated earlier. Such local frequencies are obtained by using mass-weighted coordinates in terms of which the kinetic energy is isotropic along all coordinates and hence the potential energy contains all mass and surface slope and curvature characteristics.

2.3 *Classical trajectories and cross-section evaluation*

We use a classical trajectory method and our model Hamiltonian to compute the classical *vibrational excitation* cross-section [5] as

$$\sigma_{vJ}^{A}(v_x) = \int_{b=0}^{\infty}\int_{\theta=0}^{\pi}\int_{\varphi=0}^{2\pi}\int_{\eta=0}^{2\pi}\int_{y=y_-}^{y_+}[G(Y;v,J)\,dy]\left[\frac{1}{2\pi}d\eta\right]\left[\frac{1}{2\pi}d\phi\right]$$
$$\times[\tfrac{1}{2}\sin\theta\,d\theta][2\pi b\,db]p_A(v_x, b, v, J, y, \theta, \phi, \eta),$$

where P_A is the probability of translation to vibration energy transfer, v_x is the asymptotic relative speed of A with respect to BC ($\frac{1}{2}\tilde{m}v_X^2 = E_{\text{collision}}$), the angles ϕ and θ define the BC initial orientation, η defines the BC rotation plane, b is the impact parameter, v and J are the initial vibrational and rotational quantum numbers of BC, and $G(Y; v, J)$ is the distribution function for the Y coordinate which, of course, depends on v and J. In the cases at hand, we take $v = J = 0$ and we approximate G in terms of the $v = 0$ harmonic eigenfunction for the unperturbed Y coordinate [9] $G(Y; v, J) = |\Phi_0(Y)|^2$.

For our classical simulations, we focus on near-C_{2v} collisions which therefore have small impact parameters, so we approximate P_A as

$$P_A(v_x, b, v, J, y, \theta, \phi, \eta) = \delta(\pi b^2)\delta(\eta)4\pi\delta(\phi)\delta\left(\theta - \frac{\pi}{2}\right)\delta(v)\delta(J)\frac{\text{itraj}(v_x, y)}{\text{ntraj}},$$

where ntraj is the total number of trajectories employed and itraj$(v_x, y) = 1$ or 0 depending on whether the particular collision has caused vibrational excitation or not.

Of course, to determine whether or not a collision gave rise to vibrational excitation, we had to propagate the corresponding classical trajectory. The classical Hamiltonian in mass-weighted coordinates

$$H = \tfrac{1}{2}P_X^2 + \tfrac{1}{2}P_Y^2 + \tfrac{1}{2}\omega_Y^2 Y^2 + v\exp(-\Gamma(X - KY))$$

can be used to obtain the following classical equations of motion:

$$\dot{X} = \frac{\partial H}{\partial P_X} = P_X,$$

$$\dot{P}_X = -\frac{\partial H}{\partial X} = \Gamma \cdot v \exp(-\Gamma(X - KY)),$$

$$\dot{Y} = \frac{\partial H}{\partial P_Y} = P_Y,$$

$$\dot{P}_Y = -\frac{\partial H}{\partial Y} = -\Gamma K \cdot v \exp(-\Gamma(X - KY)) - \omega_Y^2 Y.$$

We thus have a set of four coupled first-order ordinary differential equations which we chose to solve using a fifth-order Runge–Kutta scheme monitoring the local truncation error to ensure accuracy and to adjust the time step-size. We used the *Numerical Recipes* subroutines odeint, rkqs, rkck [4] to meet these needs.

For all trajectories, we set the $t = 0$ values of the coordinates and momenta as follows:

- $x = 10$ Bohr, thus $X = x\sqrt{\tilde{m}}$ (this begins all trajectories where the ion–molecule potential is negligible).
- Y and P_Y are taken to be consistent [9] with zero-point vibrational energy being in the H_2 (or D_2 or HD) molecule $\frac{1}{2}P_Y^2 + \frac{1}{2}\omega_Y^2 Y^2 = \frac{1}{2}\hbar\omega_Y$, and Y is allowed to vary between the two classical turning points with $|\Phi_0(Y)|^2$ used as a probability to generate a series of initial conditions. For each such value of Y, both positive and negative P_Y are used.
- The asymptotic (incoming) momentum along X is determined by $P_X = -\sqrt{2E_{\text{collision}}}$.
- The time duration of each trajectory is chosen to be $t_f = -\frac{3}{2}(X/P_X)_{t=0}$. If there were no interaction other than a specular reflection at $X = 0$, the time for the x coordinate to *return* to $x = 10$ Bohr would be $-2(X/P_X)_{t=0}$. Because of the repulsive interaction potential, the actual time needed to return to $x = 10$ Bohr will be less than this estimate. In practice, we found that by taking $t_f = -\frac{3}{2}(X/P_X)_{t=0}$, x had returned to and passed 10 Bohrs for all our trajectories and the total energy was found to be conserved within 10^{-4} Hartrees (i.e., to better than 0.1%).

For each collision energy, a total of 200 initial (Y, P_Y) conditions were used. At selected energies, 400 such trajectories were employed, but the vibration excitation cross-section changed little compared to the 200-trajectory results, so the smaller number was used in all the remaining cases.

In computing the cross-section, itraj(v_X, Y) is defined in terms of the number of trajectories that have $\frac{1}{2}p_Y^2 + \frac{1}{2}\omega_Y^2 Y^2 > \hbar\omega_Y$ at t_f; this is our criterion for defining the Y-mode to be in $v = 1$ or higher. To probe excitation into the $v = 1$ state alone, itraj(v_X, Y) is taken to be the number of trajectories that have $2\hbar\omega_Y \geqslant \frac{1}{2}p_Y^2 + \frac{1}{2}\omega_Y^2 Y^2 > \hbar\omega_Y$ at t_f.

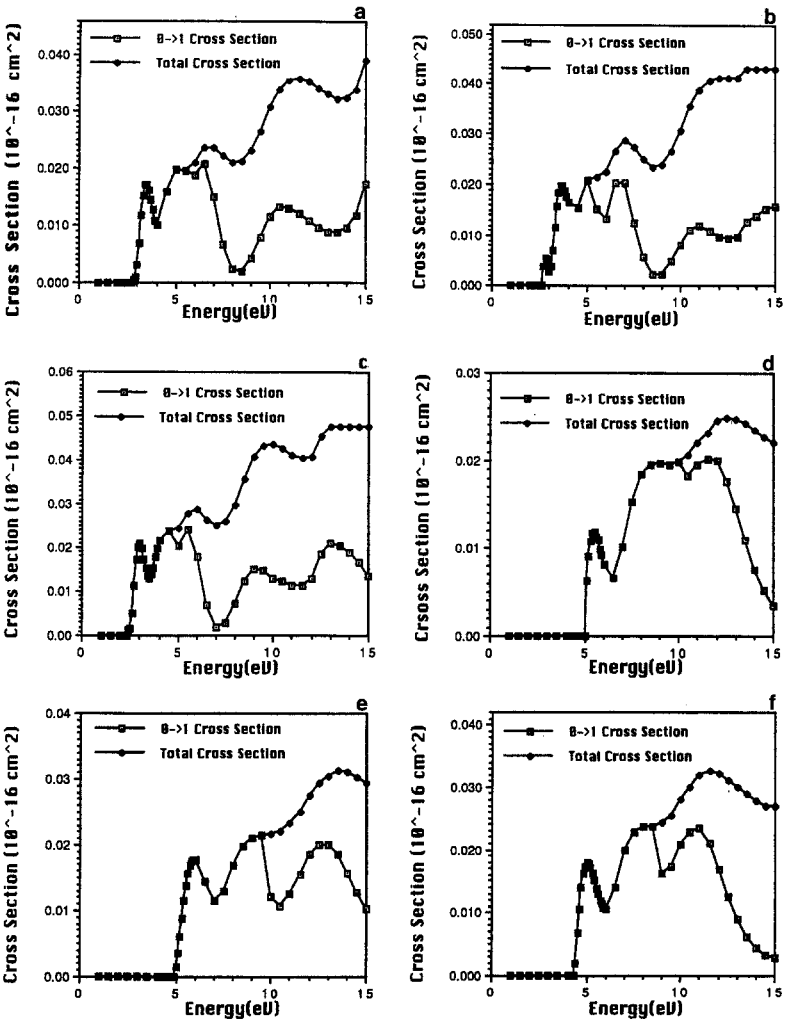

Fig. 6a–f.

2.4 *Classical trajectory results*

Figure 6a–6i shows the cross-sections for T–V energy transfer for MH_2^+, MD_2^+ and MHD_2^+ for M = B, Al, and Ga. These classically evaluated cross-sections show several noteworthy aspects:

1. For B^+, Al^+, and Ga^+ the cross-sections are indeed small (ca. 10^{-18} cm^2) and in the range of what is seen experimentally. However, the experimental trend that the cross-section is largest for B^+ and smallest for Ga^+ does not appear clearly in the classical results.
2. The T–V excitation energy thresholds for B^+, Al^+, and Ga^+ are "sharp" and do indeed greatly exceed the reaction endothermicities (which are 2.6 eV for $B^+ + H_2$,

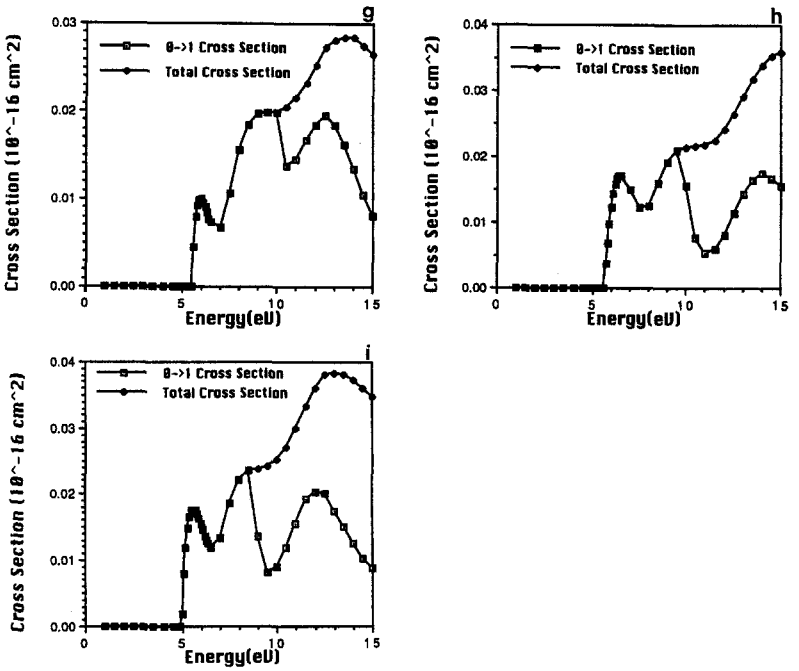

Fig. 6a. BH_2^+ cross-section. The threshold energy is 2.8 eV. The grid is 0.5 eV or better $v = 39.173 \exp(-2.81145x - 0.31132(y - y_{eq}))$; **b** BHD^+ cross-section. The threshold energy is 2.4 eV. The energy grid is 0.5 eV or better. $v = 39.173 \exp(-2.81145x - 0.31132(y - y_{eq}))$; **c** BD_2^+ cross-section. The energy threshold is 2.4 eV. The energy grid is 0.5 eV or better. $v = 39.173 \exp(-2.81145x - 0.31132(y - y_{eq}))$; **d** AlH_2^+ cross-section. The energy threshold is 5.1 eV. The energy grid is 0.5 eV or better. $v = 27.271 \exp(-2.09181x - 0.17095(y - y_{eq}))$; **e** $AlHD^+$ cross-section. The energy threshold is 5.0 eV. The energy grid is 0.5 eV or better. $v = 27.271 \exp(-2.09181x - 0.17095(y - y_{eq}))$; **f** AlD_2^+ cross-section. The energy threshold is 4.4 eV. The energy grid is 0.5 eV or better. $v = 27.271 \exp(-2.09181x - 0.17095(y - y_{eq}))$; **g** GaH_2^+ cross-section. The energy threshold is 5.6 eV. The energy grid is 0.5 eV or better. $v = 14.205 \exp(-1.72899x - 0.18944(y - y_{eq}))$; **h** GaHD cross-section. The energy threshold is 5.7 eV. The energy grid is 0.5 eV or better. $v = 14.205 \exp(-1.72899x - 0.18944(y - y_{eq}))$; **i** GaD_2^+ cross-section. The energy threshold is 5.0 eV. The energy grid is 0.5 eV or better. $v = 14.205 \exp(-1.72899x - 0.18944(y - y_{eq}))$

3.9 eV for $Al^+ + H_2$, 4.1 eV for $Ga^+ + H_2$) and lie in the neighborhoods of 3 eV for $B^+ + (D_2, HD, H_2)$, 6 eV for $Al^+ + (D_2, HD, H_2)$, and 9 eV for $Ga^+ + (D_2, HD, H_2)$, not unlike the experimental reactive thresholds. However, our classical trajectories' prediction (see Fig. 6) that the threshold energies should vary in the order $MD_2^+ < MHD^+ \approx MH_2^+$ is not seen experimentally (where $MH_2^+ \approx MD_2^+$).

3. In all $M^+ + HD$ cases, there is, of course, a single classical T–V excitation threshold energy as computed in our model. Experimentally, MD^+ is formed at lower collision energies than MH^+ when M^+ reacts with HD, so this feature of the reactive cross-sections cannot be addressed in terms of T–V energy transfer within our simple *classical* two-mode (X, Y) model. The extension of our analysis to treat the $M^+ + HD$ cases in terms of three modes is given in Sect. 3.3.

3. Quantum treatment

Although the classical trajectory numerical simulation data show similarities to what is observed experimentally, as pointed out above, not all features are accounted for. In search of reasons underlying the remaining discrepancies and to gain further insight into *why* the T–V thresholds occur where they do and are as sharp as they are, we use analytical quantum tools on the above model Hamiltonian. In particular, we do so to pursue a framework in terms of which we can better explain the various mass dependencies of the reaction cross-sections. Motivated by these desires and again keeping in mind the success of the dynamical resonance model introduced in Ref. [3], we decided to pursue an analytically soluble, rather than numerical, refinement of the model Hamiltonian used thus far.

In Ref. [3], we made use of *local* harmonic approximations to describe both the H–H (i.e., Y-mode) and M^+–H_2 (i.e., X-mode) dependencies of the potential $V(X, Y)$. Such an approach allowed us to specify, in terms of atomic masses and potential surface characteristics, the dynamical resonance conditions that permit T–V energy transfer and, by assumption, subsequent chemical reaction to occur.

In this paper, we extend the ideas from Ref. [3] and use locally defined harmonic oscillator eigenfunctions as a basis *for both the X and Y* coordinates. This may limit us to treating the *early* part of the T–V energy transfer (low Y-mode excitation) since, as shown in Figs. 2 and 5, the actual potential energy surface is harmonic only in a range of Y values (ca. $\pm$ 0.4 Bohr) near where T–V energy transfer is expected to occur. However, this approximation is appropriate if the H_2 (D_2 or HD) is initially vibrationally cold (as it is in the experiments) and if the rate-limiting step for inducing chemical reaction is the entrance-channel T–V transfer.

3.1 Local quadratic approximation to V

Focusing on the repulsive X-dependence characterizing the entrance-valley (see Fig. 2) part of V, we define

$$F(X) = V(X, Y = 0) = v \exp(-\Gamma X),$$

and approximate $F(X)$ by a *local* quadratic potential, $\tilde{F}(X)$, expanded in the neighborhood of a point X_0 in the region where the energy transfer is expected to occur from Ref. [3]. Explicitly,

$$\tilde{F}(X) = F_0 + A(X - X_0) + \tfrac{1}{2}\left(\frac{\partial^2 F}{\partial X^2}\bigg|_{X=X_0}\right)(X - X_0)^2$$

or, equivalently,

$$\tilde{F}(X) = F_0\left(1 - \frac{Z^2}{2}\right) + \tfrac{1}{2}\omega_X^2(X - X_A)^2,$$

where the parameters in $\tilde{F}$ are chosen to make

$$\frac{\partial^2 F}{\partial X^2} = \frac{\partial^2 \tilde{F}}{\partial X^2}$$

and

$$\tilde{F}(X) = F(X)$$

at X_0, thereby giving

$$F_0 = F(X_0)$$

and

$$\omega_X^2 = \Gamma^2 F_0.$$

The choice of the A parameter, or equivalently of the position X_A where the local harmonic approximation has its minimum,

$$X_A = X_0 - \frac{A}{\omega_X^2} = X_0 - \frac{Z}{\Gamma},$$

where

$$Z = \frac{\Gamma A}{\omega_X^2} = \frac{A}{\Gamma F_0},$$

implies a choice of the derivative of $\tilde{F}(X)$ at X_0.

In an independent work [6], it has been observed that equating the fitting ($\tilde{F}$) and actual (F) potentials at two points often produces a more useful fit than is obtained by equating the fitting and actual potentials and their first derivatives at a single point. Thus, it is not obvious that one wishes to choose A (i.e., Z) to cause the gradients of F and $\tilde{F}$ to be a equal at X_0.

3.1.1 Fitting $\tilde{F}$ to F at two points. In terms of the parameters entering into our local quadratic function $\tilde{F}$, fitting $\tilde{F}$ to F both at X_0 and at X_A produces the following:

$$F_0 = F(X_0)$$

and

$$\tilde{F}(X_A) = F_0\left(1 - \frac{Z^2}{2}\right) = F(X_A) = e^Z F_0.$$

The second result given above provides an equation $e^Z = (1 - Z^2/2)$ that Z (or, equivalently, the slope parameter $A = \Gamma F_0 Z$) must obey. Solutions to this equation are (i) the trivial solution, $Z = 0$ (which does not produce a second point at which $\tilde{F} = F$ since then $X_A = X_0$), and (ii) $Z = -1.176002$, which we found numerically. The value $Z = -1.176002\ldots$ is used throughout the remainder of this paper for reasons detailed shortly.

3.1.2 Fitting $\tilde{F}$ and F and first derivatives of $\tilde{F}$ and F at one point. If, alternatively, we require the slope of $\tilde{F}$ to match that of F at the single point X_0, we find

$$F_0 = F(X_0)$$

and

$$A = -\Gamma F_0.$$

The latter result implies $Z = -1.0$ rather than $Z = -1.176002$.

A comparison among the actual F potential and local quadratic approximations $\tilde{F}$ corresponding to various values of Z shows that $Z = -1.176002\ldots$ produces a potential that gives a fit satisfactory over a larger interval of X. On this basis, we have chosen the local quadratic potential provided by $Z = -1.76002$ throughout this work.

In the next section of this paper, we demonstrate that a resonance energy condition is met when ω_X and ω_Y are related by $\omega_X \cong 1.53\omega_Y$. Thus, given the ω_Y characteristic of H_2, D_2, or HD, we use this identity to compute ω_X. We then find the point X_0 at which the model potential $F = v\exp(-\Gamma X)$ has ω_X^2 as its second derivative: $X_0 = -(1/\Gamma)\ln(v\Gamma^2/\omega_X^2)$. Knowing X_0 we can evaluate $F(X_0)$. The second "contact point" X_A is then given as $X_A = X_0 - Z/\Gamma$, where $Z = -1.176002$, and the value of $F(X_A)$ is obtained as $F_0 e^Z$. As also shown in the next section, the point X_A is where our model suggests efficient energy transfer is to occur and $F(X_A)$ determines the reaction threshold.

This procedure then gives our optimal quadratic fitting function $\tilde{F} = F_0(1 - Z^2/2) + \frac{1}{2}\omega_X^2(X - X_A)^2 = F(X_A) + \frac{1}{2}\omega_X^2(X - X_A)^2$ in the neighborhood of X_A. It should be noted that this function matches the exponential F at X_0 and X_A and matches the second derivative of F at X_0 but not at X_A; the second derivative of $\tilde{F}$ at X_A is ω_X^2 while that of F at X_A is $e^Z\omega_X^2$ (i.e., at X_A the local harmonic frequency of the actual F function is $\sqrt{e^Z} = 0.85$ of its value at X_0, which we express as $\omega(X_A) = 0.85\omega_X$).

3.2 Resonances in first-order solution of the Schrödinger equation

Treating $V(X, Y) - \tilde{F}(X)$, which includes X–Y-mode coupling and non-harmonic X-character of V as a perturbation ΔV, we now express the quantum dynamics on the full $V(X, Y) + \frac{1}{2}\omega_Y^2 Y^2$ surface in terms of approximate dynamics on the $\tilde{F}(X) + \frac{1}{2}\omega_Y^2 Y^2$ fit potential surface. We begin by rewriting the Schrödinger equation for the two-dimensional Hamiltonian as

$$\left\{-\frac{\hbar^2}{2}\frac{\partial^2}{\partial Q^2} + F(X_A) + \tfrac{1}{2}\omega_X^2 Q^2 - \frac{\hbar^2}{2}\frac{\partial^2}{\partial Y^2} + \tfrac{1}{2}\omega_Y^2 Y^2 - E\right\}\Psi(Q, Y) = -\Delta V(Q, Y)\Psi(Q, Y),$$

where

$$Q = X - X_A$$

is the displacement along the X coordinate from the point X_A at which $\tilde{F} = F = F_A$, and near where

$$\tilde{F}(Q) = F_A + \tfrac{1}{2}\omega_X^2 Q^2.$$

In terms of the displacement coordinates Q and Y, the perturbation occurring on the right side of the Schrödinger equation is written as

$$-\Delta V(Q, Y) = \tilde{F}(Q) - V(X, Y) = F_A + \tfrac{1}{2}\omega_X^2 Q^2 - F_A e^{-\Gamma(Q - KY)}.$$

The eigenvectors $\Psi(Q, Y)$ of the full Hamiltonian involving $V(X, Y)$ can be expanded in terms of the eigenfunctions $\{\Phi_n(Q)\Phi_M(Y)\}$ of the left-hand side of the Schrödinger equation as

$$\Psi(Q, Y) = \sum_{n=0}^{\infty}\sum_{M=0}^{\infty}\Phi_n(Q)\Phi_M(Y)C_{nM},$$

where

$$\Phi_n(Q) = \frac{1}{\sqrt{2^n n!}}\left(\frac{\omega_X}{\hbar\pi}\right)^{1/4}\exp\left(-\frac{\omega_X}{2\hbar}Q^2\right)H_n\left(Q\sqrt{\frac{\omega_X}{\hbar}}\right)$$

and

$$\Phi_M(Y) = \frac{1}{\sqrt{2^M M!}}\left(\frac{\omega_Y}{\hbar\pi}\right)^{1/4} \exp\left(-\frac{\omega_Y}{2\hbar}Y^2\right) H_M\left(Y\sqrt{\frac{\omega_Y}{\hbar}}\right)$$

are the conventional harmonic oscillator functions of Q and Y, and C_{nM} are expansion coefficients.

To model the entrance-channel *initial* state of the M^+–H_2 system, we specify the quantum number (I) for the Y-mode describing the H–H vibration as well as a quantum number (i) relating to the initial energy content of the X-mode. These quantum numbers thus specify an initial (unperturbed) eigenvector $\Psi^0(Q, Y) \approx \Phi_i(Q)\Phi_I(Y)$, and an initial zeroth-order energy

$$E^0_{i,I} = F_A + \hbar\omega_X(i + \tfrac{1}{2}) + \hbar\omega_Y(I + \tfrac{1}{2}).$$

Because we wish to formulate solutions $\Psi(Q, Y)$ in terms of a perturbation that induces *transitions* $i, I \to n, M$ but not energy shifts, we add to both sides of the above Schrödinger equation the average value ΔV_{iI} of ΔV for the specific i, I initial state of interest:

$$\Delta V_{iI} = \langle \Phi_i(Q)\Phi_I(Y)|\Delta V(Q, Y)|\Phi_i(Q)\Phi_I(Y)\rangle.$$

It can be shown (using the expressions on p. 60 of Ref. [7]) that this average value can be expressed as follows:

$$\begin{aligned} -\Delta V_{iI} = {} & [F_A + \tfrac{1}{2}(i + \tfrac{1}{2})\hbar\omega_X] \\ & - F_A\left[e^{\hbar\Gamma^2/4\omega_X}\sum_{k=0}^{i}\frac{i!}{(k!)^2(i-k)!}\left(\frac{\hbar\Gamma^2}{2\omega_X}\right)^k\right] \\ & \times\left[e^{\hbar K^2\Gamma^2/4\omega_Y}\sum_{L=0}^{I}\frac{I!}{(L!)^2(I-L)!}\left(\frac{\hbar K^2\Gamma^2}{2\omega_Y}\right)^L\right]. \end{aligned}$$

To clarify the physical content of this energy shift, expansions in powers of K^2 and Γ^2K^2/ω_Y can be carried out (see Table 3, where it is shown that these parameters are $\ll 1.0$). The lowest-order terms thus obtained are:

$$\begin{aligned} -\Delta V_{iI} &= F_A + \tfrac{1}{2}\hbar\omega_X(i + \tfrac{1}{2}) \\ &\quad - F_A\left[1 + \frac{\frac{1}{2}\Gamma^2}{\omega_X^2}\hbar\omega_X(i + \tfrac{1}{2}) + \frac{\frac{1}{2}K^2\Gamma^2}{\omega_Y^2}\hbar\omega_Y(I + \tfrac{1}{2}) + \cdots\right] \\ &\cong \tfrac{1}{2}\hbar\omega_X(i + \tfrac{1}{2}) - \tfrac{1}{2}\hbar\omega_X(i + \tfrac{1}{2})\left(\frac{F_A\Gamma^2}{\omega_X^2}\right) \\ &\quad - \tfrac{1}{2}\hbar\omega_Y(I + \tfrac{1}{2})\frac{F_A\Gamma^2}{\omega_Y^2}K^2 + \cdots. \end{aligned}$$

Recalling that $\omega_X^2 = \Gamma^2 F_0$ and that $F_A/F_0 = e^z = 0.31$ we find

$$-\Delta V_{iI} \cong \tfrac{1}{2}\hbar\omega_X(i + \tfrac{1}{2})(1 - e^z) - \tfrac{1}{2}\hbar\omega_Y(I + \tfrac{1}{2})\frac{K^2e^z\omega_X^2}{\omega_Y^2}.$$

So, the i, I diagonal element of ΔV produces a shift in the X-mode *potential* energy related to the change in the curvature along that mode from ω_X^2 at X_0 to $\omega^2(X_A) = e^z\omega_X^2$ at X_A. This diagonal element also involves a (smaller, because it is proportional to K^2) change in the Y-mode potential energy.

Defining the energy ε relative to the bottom of the harmonic potential (F_A) plus the "shift" induced by ΔV_{iI}.

$$\varepsilon = E - F_A - \Delta V_{iI}.$$

we can rewrite the Schrödinger equation with a right-hand side that causes only transitions but no further shift in the initial state's energy:

$$\left\{ -\frac{\hbar^2}{2}\frac{\partial^2}{\partial Q^2} + \tfrac{1}{2}\omega_X^2 Q^2 - \frac{\hbar^2}{2}\frac{\partial^2}{\partial Y^2} + \tfrac{1}{2}\omega_Y^2 Y^2 - \varepsilon \right\} \Psi(Q, Y)$$
$$= (-\Delta V + \Delta V_{iI})\Psi(Q, Y).$$

The Green function of the left-hand side of this Schrödinger equation is

$$G(Q, Y; Q', Y') = \sum_{n=0}^{\infty}\sum_{M=0}^{\infty} \frac{\Phi_n(Q)\Phi_M(Y)\Phi_n^*(Q')\Phi_M^*(Y')}{(n+\frac{1}{2})\hbar\omega_X + (M+\frac{1}{2})\hbar\omega_Y - \varepsilon},$$

and the integral equation equivalent to the above Schrödinger equation and its boundary conditions is

$$\Psi(Q, Y) = \Psi^0(Q, Y) + \int dQ'\, dY'\, G(Q, Y; Q', Y')[\Delta V_{iI} - \Delta V](Q', Y')\Psi(Q', Y').$$

Strong contributions to the above integral over Y' and Q' are expected whenever ε approaches $(n+\frac{1}{2})\hbar\omega_X + (M+\frac{1}{2})\hbar\omega_Y$.

The relative importance of each such "resonance" (i.e., each such n, M pair) is determined by the magnitude of the matrix elements $\langle \Phi_n\Phi_M|\Delta V|\Phi_i\Phi_I\rangle$, and the T–V excitations threshold is determined by the lowest value of E at which a strong resonance can occur.

We know from our classical trajectory simulations that $\Delta v = 1$ processes are dominant in the T–V excitation, especially near threshold, so we can anticipate that the first-order correction to Ψ^0 obtained as the first iterate of this integral equation,

$$\Psi^1(Q, Y) = \int dQ'\, dY'\, G(Q, Y; Q', Y')[\Delta V_{iI} - \Delta V](Q', Y')\Psi^0(Q', Y'),$$

should embody the primary effects for our system in the threshold energy regime. Because our zeroth-order wave function is of the form

$$\Psi^0(Q, Y) = \Phi_i(Q)\Phi_I(Y),$$

with $I = 0$ (because the hydrogen molecules are initially vibrationally cold), the first-order wavefunction correction can be written explicitly as

$$\Psi^1(Q, Y) = \sum_{(n, M)\neq(i, I)} \left\{ \frac{\Phi_n(Q)\Phi_M(Y)}{(n+\frac{1}{2})\hbar\omega_X + (M+\frac{1}{2})\hbar\omega_Y - \varepsilon} \right\}$$
$$\times \left\{ \frac{\hbar\omega_X}{4}[\delta_{n,i+2}\sqrt{n(n-1)} + \delta_{n,i-2}\sqrt{(n+1)(n+2)}]\delta_{M,I} \right.$$
$$\left. - F_A\left[\frac{1}{\sqrt{2^n n!}} \frac{1}{\sqrt{2^i i!}} e^{\hbar\Gamma^2/4\omega_X} \left(-\Gamma\sqrt{\frac{\hbar}{\omega_X}} \right)^{i+n} \right.\right.$$

$$\times \sum_{j=0}^{\min(i,n)} \frac{n!i!}{j!(n-j)!(i-j)!}\left(\frac{2\omega_X}{\hbar\Gamma^2}\right)^j\Bigg]$$

$$\times\Bigg[\frac{1}{\sqrt{2^M M!}}\frac{1}{\sqrt{2^I I!}}\,e^{\hbar K^2\Gamma^2/4\omega_Y}\left(K\Gamma\sqrt{\frac{\hbar}{\omega_X}}\right)^{I+M}$$

$$\times \sum_{J=0}^{\min(I,M)} \frac{M!I!}{J!(M-J)!(I-J)!}\left(\frac{2\omega_Y}{\hbar K^2\Gamma^2}\right)^J\Bigg]\Bigg\}.$$

The resonance condition relating ω_X and ω_Y outlined in the preceding section is obtained by requiring that $\Delta v = 1$ single-quantum T–V energy exchange be resonant for the $1, 0 \leftarrow 0, 1$ process. It can be shown that the expectation value of the model Hamiltonian in our basis is

$$\begin{aligned} E_{nM} &= \langle \Phi_n(Q)\Phi_M(Y)|H|\Phi_n(Q)\Phi_M(Y)\rangle \\ &= (M+\tfrac{1}{2})\hbar\omega_Y + \tfrac{1}{2}(n+\tfrac{1}{2})\hbar\omega_X \\ &+ F_A e^{(-\hbar\Gamma^2/4\omega_X - \hbar\Gamma^2K^2/4\omega_Y)}\left\{\sum_{j=0}^{n}\frac{n!}{(n-j)!(j!)^2}\left(\frac{\hbar\Gamma^2}{2\omega_X}\right)^j\right\} \\ &\times\left\{\sum_{L=0}^{M}\frac{M!}{(M-L)!(L!)^2}\left(\frac{\hbar\Gamma^2K^2}{2\omega_Y}\right)^L\right\}. \end{aligned}$$

Thus

$$E_{1,0} = \tfrac{1}{2}\hbar\omega_Y + \tfrac{1}{2}(1+\tfrac{1}{2})\hbar\omega_X + F_A e^{(-\hbar\Gamma^2/4\omega_X - \hbar\Gamma^2K^2/4\omega_Y)}\left(1+\frac{\hbar\Gamma^2}{2\omega_X}\right)$$

and

$$E_{0,1} = (1+\tfrac{1}{2})\hbar\omega_Y + \tfrac{1}{4}\hbar\omega_X + F_A e^{(-\hbar\Gamma^2/4\omega_X - \hbar\Gamma^2K^2/4\omega_Y)}\left(1+\frac{\hbar\Gamma^2K^2}{2\omega_Y}\right).$$

The identity $E_{10} = E_{01}$ can then be solved for ω_X in terms of ω_Y, with the result

$$\frac{\omega_X}{\omega_Y} \approx \frac{2+(\hbar\Gamma^2/4\omega_Y)e^z}{1+e^z} \approx \frac{2}{1+e^z} = 1.53.$$

Thus, optimal T–V energy transfer should occur at geometries where $\omega_X \cong 1.53\omega_Y$, according to this model. In practice, this resonance condition directs us to seek regions of the potential surface (X_0) near which $\omega_X = 1.53\omega_Y$. The repulsion energy F_0 at this geometry then gives the surface's range parameter $\Gamma = \omega_X^2/F_0$, which allows the geometry $X_A = X_0 + 1.176/\Gamma$, where the local potential surface curvature $\omega(X_A) = (0.85)\,(1.53)\,\omega_Y = 1.30\omega_Y$, to be computed.

The relation between the repulsion energy F_A at X_A and the threshold collision energy $E_{\text{collision}}$ necessary to achieve facile T–V energy transfer can be seen by examining the energy dependence of the multitude of terms contributing to $\Psi^1(Q, Y)$.In particular, the denominator relating to the $0, 1 \rightarrow 1, 0$ process can be expressed in terms of the total collision energy E as

$$-\tfrac{1}{4}\hbar\omega_X + \tfrac{3}{2}\hbar\omega_Y + F_A\left(1+\frac{\hbar\Gamma^2}{2\omega_X}\right)\exp\left(\frac{\hbar\Gamma^2}{4\omega_X}+\frac{\hbar K^2\Gamma^2}{4\omega_Y}\right) - E.$$

Table 4. Values for the X-mode frequency, F_0, F_A, X_0, and X_A

	$\omega_X = \frac{2}{1+e^z}\omega_Y$	F_0(a.u.)	F_A(a.u.)	x_0(Bohr)	x_A(Bohr)
BH_2^+	0.0306 (0.83 eV)	0.3686 (10.03 eV)	0.1137 (3.09 eV)	1.6596 (0.878 Å)	2.0779 (1.099 Å)
BHD^+	0.0266 (0.72 eV)	0.3881 (10.55 eV)	0.1197 (3.25 eV)	1.6413 (0.868 Å)	2.0596 (1.090 Å)
BD_2^+	0.0217 (0.59 eV)	0.3210 (8.73 eV)	0.0990 (2.69 eV)	1.7088 (0.904 Å)	2.1271 (1.126 Å)
AlH_2^+	0.0306 (0.83 eV)	0.7306 (19.88 eV)	0.2254 (6.13 eV)	1.730 (0.916 Å)	2.293 (1.213 Å)
$AlHD^+$	0.0266 (0.72 eV)	0.8021 (21.83 eV)	0.2475 (6.73 eV)	1.686 (0.892 Å)	2.248 (1.189 Å)
AlD_2^+	0.0217 (0.59 eV)	0.6912 (18.81 eV)	0.2133 (5.80 eV)	1.757 (0.930 Å)	2.319 (1.227 Å)
GaH_2^+	0.0306 (0.83 eV)	1.1211 (30.51 eV)	0.3459 (9.41 eV)	1.4686 (0.777 Å)	2.1488 (1.137 Å)
$GaHD^+$	0.0266 (0.72 eV)	1.2491 (33.99 eV)	0.3854 (10.48 eV)	1.4061 (0.744 Å)	2.0862 (1.104 Å)
GaD_2^+	0.0217 (0.59 eV)	1.0989 (29.90 eV)	0.3390 (9.22 eV)	1.480 (0.783 Å)	2.1604 (1.143 Å)

Table 5. Comparison between our quantum and classical model predictions and those from the mass-weighted Hessian eigenvalues and experimental thresholds. All the energies are in eV, and all distances are in Å

Species	F_A	x_A	E_{CM}	R_{cross} [3]	E_{cross} [3]	ΔE_{ther} [3]	E_{exp} [3]
$B^+ + HH$	3.09	1.10	> 2.8	> 1.05	< 3.9	2.6	3.3 ± 0.1
$B^+ + HD$	3.25	1.10	> 2.4	> 1.00; MD	< 4.6		4.0 ± 0.2
				> 1.05; MH	< 3.9		3.0 ± 0.2
$B^+ + DD$	2.69	1.13	> 2.4	> 1.05	< 3.9		3.3 ± 0.1
$Al^+ + HH$	6.13	1.21	> 5.1	> 1.22	< 6.4		6.6 ± 0.2
$Al^+ + HD$	6.73	1.19	> 5.0	> 1.16; MD	< 7.7	3.9	6.7 ± 0.1
				> 1.22; MH	< 6.4		4.7 ± 0.1
$Al^+ + DD$	5.80	1.23	> 4.4	> 1.22	< 6.4		6.6 ± 0.1
$Ga^+ + HH$	9.41	1.14	> 5.6	> 1.21	< 7.4		NA
$Ga^+ + HD$	10.48	1.10	> 5.7	> 1.15; MD	< 9.0	4.1	NA
				> 1.25; MH	< 6.3		
$Ga^+ + DD$	9.22	1.14	> 5.0	> 1.21	< 7.4		8.5 ± 0.5

Since $\omega_X \cong 1.5\,\omega_Y$ and because $\hbar\Gamma^2/\omega_X$ and $\hbar\Gamma^2K^2/\omega_Y$ are $\ll 1$ (see Tables 3 and 4), this denominator will become small when $E \cong F_A$. For this reason, we can predict threshold energies once $F(X_A)$ is obtained.

For all of the reactions studied, our primary findings (the predicted threshold energies F_A) are summarized in Tables 4 and 5 and compared in Table 5 to our classical T–V energy transfer onset (E_{class}), the experimentally observed reaction

threshold energies (E_{exp}), the endothermicities (E_{ther}), and the threshold predictions of our earlier works (E_{cross}).

Although our F_A thresholds, which are based on using our model's prediction of T–V energy transfer onset as the chemical reaction onset, display the general trends of the experimental thresholds they still are not in quantitative agreement and they do not differentiate between MD^+ and MH^+ thresholds in the HD case.

3.3 *Asymmetry in the MD^+/MH^+ thresholds*

Once collisional energy has been deposited into the B–C vibrational motion, the possibility of forming MH^+ or MD^+ product ions is assumed to be non-negligible in our model. For $M^+ + H_2$ or $M^+ + D_2$ collisions, only MH^+ or MD^+ respectively, can be formed. However, in the $M^+ + HD$ case, a new issue arises; it remains to be explained why MD^+ is formed at (significantly) lower collision energies than MH^+.

We begin our analysis of this aspect of the reaction by introducing the following three-atom classical Hamiltonian:

$$H = T + U,$$

where the kinetic energy is written in terms of the three masses and velocities as

$$T = \tfrac{1}{2}m_A\dot{r}_A^2 + \tfrac{1}{2}m_B\dot{r}_B^2 + \tfrac{1}{2}m_C\dot{r}_C^2$$

and the internal potential energy is assumed to be locally represented as a sum of quadratic functions of the three interatomic distances

$$U = \tfrac{1}{2}k_{BC}(r_B - r_C - r_{BC}^{eq})^2 + \tfrac{1}{2}k_{AB}(r_A - r_B - r_{AB}^{eq})^2 + \tfrac{1}{2}k_{AC}(r_A - r_C - r_{AC}^{eq})^2.$$

We next transform to a coordinate system involving the center of mass coordinate of the three atoms r_{CM} and two relative position vectors $\boldsymbol{x}$ and $\boldsymbol{y}$ as shown in Fig. 7.

Expressing T and U in terms of these three new vector coordinates, we obtain

$$T = \tfrac{1}{2}\tilde{m}\dot{\boldsymbol{x}}^2 + \tfrac{1}{2}\mu\dot{\boldsymbol{y}}^2 + \tfrac{1}{2}M\dot{r}_{CM}^2,$$

$$U = \tfrac{1}{2}k_{BC}(\boldsymbol{y} - \boldsymbol{r}_{BC}^{eq})^2 + \tfrac{1}{2}k_{AB}\left(\boldsymbol{x} - \frac{\mu}{m_B}\boldsymbol{y} - \boldsymbol{r}_{AB}^{eq}\right)^2 + \tfrac{1}{2}k_{AC}\left(\boldsymbol{x} + \frac{\mu}{m_C}\boldsymbol{y} - \boldsymbol{r}_{AC}^{eq}\right)^2,$$

where the effective masses $\tilde{m}$ and μ are as employed earlier in this paper and $M = m_A + m_B + m_C$. Now introducing mass-weighted coordinates

$$\boldsymbol{Y} = \sqrt{\mu}(\boldsymbol{y} - \boldsymbol{y}_{eq}),$$

$$\boldsymbol{X} = \sqrt{\tilde{m}}(\boldsymbol{x} - \boldsymbol{x}_{eq}),$$

where

$$\boldsymbol{y}_{eq} = \boldsymbol{r}_{BC}^{eq}$$

and

$$\boldsymbol{x}_{eq} = \boldsymbol{r}_{AB}^{eq} - \frac{\mu}{m_B}\boldsymbol{r}_{BC}^{eq} = \boldsymbol{r}_{AC}^{eq} + \frac{\mu}{m_C}\boldsymbol{r}_{BC}^{eq},$$

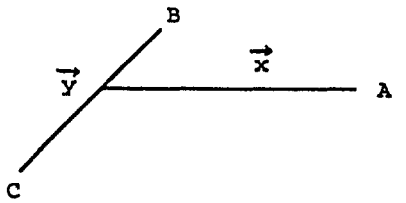

Fig. 7. Internal coordinate system

we are able to write H in a manner reminiscent of the Hamiltonian used earlier in Sect. 2, except that X and Y are vectors in a plane.

$$T = \tfrac{1}{2}\dot{X}^2 + \tfrac{1}{2}\dot{Y}^2 + \tfrac{1}{2}M\dot{r}_{CM}^2,$$

$$U = \tfrac{1}{2}\varpi_Y^2 Y^2 + \tfrac{1}{2}\varpi_X^2 X^2 - \delta X \cdot Y.$$

Clearly, the center of mass coordinate propagates independently, so it can be removed from further consideration. The ϖ_Y and ϖ_X frequencies, which need not be identical to the ω_X and ω_Y used earlier in this paper, are expressed in terms of the force constant parameters defining U and the pertinent masses as follows:

$$\varpi_Y^2 = \left(\frac{k_{BC}}{\mu} + \left(\frac{\mu}{m_B}\right)^2 \frac{k_{AB}}{\mu} + \left(\frac{\mu}{m_C}\right)^2 \frac{k_{AC}}{\mu}\right).$$

$$\varpi_X^2 = \left(\frac{k_{AB}}{\tilde{m}} + \frac{k_{AC}}{\tilde{m}}\right),$$

and the parameter δ governing the strength of the X and Y coupling is given by

$$\delta = \sqrt{\frac{\mu}{\tilde{m}}}\left(\frac{k_{AB}}{m_B} - \frac{k_{AC}}{m_C}\right).$$

In the $M^+ + H_2$ and $M^+ + D_2$ cases, the δ parameter vanishes.

We can rewrite the potential as a quadratic form

$$U(X, Y) = (X, Y)\begin{pmatrix} \frac{\varpi_X^2}{2} & -\frac{\delta}{2} \\ -\frac{\delta}{2} & \frac{\varpi_Y^2}{2} \end{pmatrix}\begin{pmatrix} X \\ Y \end{pmatrix}$$

involving a matrix

$$\begin{pmatrix} \frac{\varpi_X^2}{2} & -\frac{\delta}{2} \\ -\frac{\delta}{2} & \frac{\varpi_Y^2}{2} \end{pmatrix}$$

whose eigenvalues are

$$\omega_{\mp}^2 = \tfrac{1}{2}(\varpi_X^2 + \varpi_T^2) \mp s,$$

where

$$s = \tfrac{1}{2}\sqrt{(\varpi_X^2 - \varpi_Y^2)^2 + 4\delta^2}.$$

The corresponding two eigenvectors of the above matrix allow the normal mode displacement vectors of the coupled system to be written as

$$\begin{pmatrix}\eta_- \\ \eta_+\end{pmatrix} = \begin{pmatrix} +\sqrt{\frac{1}{2}+\frac{1}{2}\left(\frac{\varpi_Y^2-\varpi_X^2}{\omega_+^2-\omega_-^2}\right)} & +\sqrt{\frac{1}{2}-\frac{1}{2}\left(\frac{\varpi_Y^2-\varpi_X^2}{\omega_+^2-\omega_-^2}\right)} \\ -\sqrt{\frac{1}{2}-\frac{1}{2}\left(\frac{\varpi_Y^2-\varpi_X^2}{\omega_+^2-\omega_-^2}\right)} & +\sqrt{\frac{1}{2}+\frac{1}{2}\left(\frac{\varpi_Y^2-\varpi_X^2}{\omega_+^2-\omega_-^2}\right)} \end{pmatrix} \begin{pmatrix} X \\ Y \end{pmatrix}.$$

The AB and AC interatomic distances can be written in terms of X and Y as

$$\begin{pmatrix} R_{AB} \\ R_{AC}\end{pmatrix} = \begin{pmatrix} \frac{1}{\sqrt{\tilde{m}}} & -\frac{\mu}{m_B}\frac{1}{\sqrt{\mu}} \\ \frac{1}{\sqrt{\tilde{m}}} & \frac{\mu}{m_C}\frac{1}{\sqrt{\mu}} \end{pmatrix} \begin{pmatrix} X \\ Y \end{pmatrix},$$

where

$$R_{AB} = r_{AB} - r_{AB}^{eq}$$

and

$$R_{AC} = r_{AC} - r_{AC}^{eq}.$$

Then using the above expressions for the eigenmodes, these same interatomic distances can be rewritten as

$$\begin{pmatrix} R_{AB} \\ R_{AC}\end{pmatrix} = \begin{pmatrix} \frac{1}{\sqrt{\tilde{m}}} & -\frac{\mu}{m_B}\frac{1}{\sqrt{\mu}} \\ \frac{1}{\sqrt{\tilde{m}}} & \frac{\mu}{m_C}\frac{1}{\sqrt{\mu}} \end{pmatrix} \times \begin{pmatrix} +\sqrt{\frac{1}{2}+\frac{1}{2}\left(\frac{\varpi_Y^2-\varpi_X^2}{\omega_+^2-\omega_-^2}\right)} & -\sqrt{\frac{1}{2}-\frac{1}{2}\left(\frac{\varpi_Y^2-\varpi_X^2}{\omega_+^2-\omega_-^2}\right)} \\ +\sqrt{\frac{1}{2}-\frac{1}{2}\left(\frac{\varpi_Y^2-\varpi_X^2}{\omega_+^2-\omega_-^2}\right)} & +\sqrt{\frac{1}{2}+\frac{1}{2}\left(\frac{\varpi_Y^2-\varpi_X^2}{\omega_+^2-\omega_-^2}\right)} \end{pmatrix} \begin{pmatrix} \eta_- \\ \eta_+ \end{pmatrix}.$$

In terms of the $\eta_\pm$ vectors, the Hamiltonian becomes

$$H = T + U = \tfrac{1}{2}\dot{\eta}_-^2 + \tfrac{1}{2}\omega_-^2\eta_-^2 + \tfrac{1}{2}\dot{\eta}_+^2 + \tfrac{1}{2}\omega_+^2\eta_+^2.$$

In the remaining portion of this analysis, we proceed as follows:

(i) We assume that once the total collision energy E reaches the range $F(X_A)$ where appreciable T–V energy transfer begins, the subsequent dynamical evolution of the three-atom system is best represented in terms of time evolution of the local *normal* modes ($\eta_\pm$).

(ii) We partition the total energy E in excess of $F(X_A)$ between the two normal modes $E = F(X_A) + E_+ + E_-$, with $E_+ = \langle \tfrac{1}{2}\dot{\eta}_+^2 + \tfrac{1}{2}\omega_+^2\eta_+^2 \rangle$ and $E_- = \langle \tfrac{1}{2}\dot{\eta}_-^2 + \tfrac{1}{2}\omega_-^2\eta_-^2 \rangle$ describing the energy content of the two modes.

(iii) We then use equipartition [8] of the *excess* energy (e.g., assuming adequate time to permit appreciable randomization of the energy $E - F(X_A)$ in excess of the

lowest threshold) to relate the mean square A–B and A–C interatomic displacements $\langle R_{AB}^2 \rangle$ and $\langle R_{AC}^2 \rangle$, to $\langle \eta_\pm^2 \rangle$ and hence to $E - F(X_A)$.
(iv) We show that, in the BC = HD case, $\langle R_{AH}^2 \rangle$ is greater than $\langle R_{AD}^2 \rangle$ for any $E > F(X_A)$. This observation is used to infer that a lower collision energy is required to eject the H atom (thus leaving AD^+) from this energized three-atom complex. Hence the threshold for MD^+ formation should occur at lower total energies than that for MH^+ formations.

1. H_2 and D_2 cases. Let us first consider the $M^+ + H_2$ and $M^+ + D_2$ cases where $m_B = m_C = m_H$ for H_2 and $m_B = m_C = 2m_H$ for D_2, and for which $\delta = 0$, allowing considerable simplification in the above expressions. In particular, now

$$\begin{pmatrix} \eta_- \\ \eta_+ \end{pmatrix} = \begin{pmatrix} X \\ Y \end{pmatrix},$$

$$\omega_-^2 = \varpi_X^2 = \frac{2k}{\tilde{m}},$$

$$\omega_+^2 = \varpi_Y^2 = \frac{k_{BC}}{\mu} + \tfrac{1}{2}\frac{k}{\mu}$$

and

$$\begin{pmatrix} R_{AB} \\ R_{AC} \end{pmatrix} = \begin{pmatrix} \dfrac{1}{\sqrt{\tilde{m}}} & -\dfrac{1}{2\sqrt{2\mu}} \\ \dfrac{1}{\sqrt{\tilde{m}}} & +\dfrac{1}{2\sqrt{2\mu}} \end{pmatrix} \begin{pmatrix} \eta_- \\ \eta_+ \end{pmatrix}.$$

The average values of $\langle R_{AB}^2 \rangle$ and $\langle R_{AC}^2 \rangle$ can be expressed in terms of those of $\langle \eta_\pm \rangle$:

$$\langle R_{AB}^2 \rangle = \frac{1}{\tilde{m}}\langle \eta_-^2 \rangle - \frac{1}{\sqrt{2\tilde{m}\mu}}\langle \eta_- \cdot \eta_+ \rangle + \frac{1}{8\mu}\langle \eta_+^2 \rangle,$$

$$\langle R_{AC}^2 \rangle = \frac{1}{\tilde{m}}\langle \eta_-^2 \rangle + \frac{1}{\sqrt{2\tilde{m}\mu}}\langle \eta_- \cdot \eta_+ \rangle + \frac{1}{8\mu}\langle \eta_+^2 \rangle,$$

and $\langle \eta_- \cdot \eta_+ \rangle = 0$.

From equipartition of energy

$$\tfrac{1}{2}\omega_-^2 \langle \eta_-^2 \rangle = \tfrac{1}{2}E_- = \tfrac{1}{2}\hbar\omega_- \eta_-^{\text{eff}},$$

$$\tfrac{1}{2}\omega_+^2 \langle \eta_+^2 \rangle = \tfrac{1}{2}E_+ = \tfrac{1}{2}\hbar\omega_+ \eta_+^{\text{eff}},$$

where $\eta_\pm^{\text{eff}}$ are quantum numbers describing the energy and momentum content of the two local normal modes (specifically, the energy content *above* the "bottom" $F(X_A)$ of the local harmonic potential). We thus obtain

$$\langle R_{AB}^2 \rangle = \langle R_{AC}^2 \rangle = \frac{1}{\tilde{m}}\hbar\omega_-^{-1}\eta_-^{\text{eff}} + \frac{1}{8\mu}\hbar\omega_+^{-1}\eta_+^{\text{eff}}.$$

Since $k_{AB} = k_{AC} = k$ we can rewrite these results as

$$\langle R_{AB}^2 \rangle = \langle R_{AC}^2 \rangle = \frac{\hbar\eta_-^{\text{eff}}}{\sqrt{2k\tilde{m}}} + \frac{\hbar\eta_+^{\text{eff}}}{8\sqrt{(k + k_{BC})\mu}}.$$

For H_2 and D_2, $\mu = \frac{1}{2}m_H$ and $\mu = m_H$, respectively, and $\tilde{m} = m_A(m_B + m_C)/(m_A + m_B + m_C) \approx 2m_H$ and $\tilde{m} = 4m_H$, respectively. Hence for H_2

$$\langle R_{AH}^2 \rangle = \frac{\hbar\eta_-^{\text{eff}}}{\sqrt{4km_H}} + \frac{\sqrt{2}\hbar\eta_+^{\text{eff}}}{8\sqrt{(k + k_{BC})m_H}},$$

while for D_2

$$\langle R_{AD}^2 \rangle = \frac{\hbar\eta_-^{\text{eff}}}{\sqrt{8km_H}} + \frac{\hbar\eta_+^{\text{eff}}}{8\sqrt{(k + k_{BC})m_H}}.$$

Thus for any given energy E in excess $F(X_A)$ characterized by η_I^{eff}, $\langle R_{AH}^2 \rangle$ will be larger than $\langle R_{AD}^2 \rangle$.

Recall that our classical trajectory simulations showed somewhat lower T–V *energy transfer thresholds for* $M^+ + D_2$ than for $M^+ + H_2$, whereas the experimental *reaction* thresholds seem to be much closer for D_2 and H_2. The results of the preceding paragraph imply that, although $M^+ + D_2$ collisions may lead to T–V excitation at lower E, it will require more excess energy (i.e., higher $\eta_\pm^{\text{eff}}$) to cause $\langle R_{MD}^2 \rangle$ to exceed a "critical bond breaking" distance. For $M^+ + H_2$, T–V excitation requires more collision energy, but for $\langle R_{MH}^2 \rangle$ to then exceed the critical value, less *excess* energy (i.e., smaller $\eta_\pm^{\text{eff}}$) is needed. The net effects is that these two competing tendencies essentially cancel, thus rendering the H_2 and D_2 *reactive* thresholds very similar.

2. The HD case. We define $m_C = m_H$ and $m_B = m_D = 2m_H$, as a result of which $\mu = \frac{2}{3}m_H$, $\varpi_Y^2 = k_{HD}/\mu + \frac{5}{6}k/m_H$, $\varpi_X^2 = 2k/\tilde{m}$, $\delta = -\frac{1}{2}\sqrt{(\tilde{m}/6m_H)}\,\varpi_X^2$ and noticing that $\varpi_X \ll \varpi_Y$ and $\delta \ll \varpi_Y$, we obtain

$$\omega_-^2 \approx \varpi_X^2 - \frac{\delta^2}{\varpi_Y^2 - \varpi_X^2},$$

$$\omega_+^2 \approx \varpi_Y^2 - \frac{\delta^2}{\varpi_Y^2 - \varpi_X^2},$$

$$2\tilde{m}\langle R_{AB}^2 \rangle = \left(\sqrt{1 + \left(\frac{\varpi_Y^2 - \varpi_X^2}{\omega_+^2 - \omega_-^2} \right)} - \frac{\mu}{m_B}\sqrt{\frac{\tilde{m}}{\mu}}\sqrt{1 - \left(\frac{\varpi_Y^2 - \varpi_X^2}{\omega_+^2 - \omega_-^2} \right)} \right)^2 \langle \eta_-^2 \rangle$$

$$+ \left(-\sqrt{1 - \left(\frac{\varpi_Y^2 - \varpi_X^2}{\omega_+^2 - \omega_-^2} \right)} - \frac{\mu}{m_B}\sqrt{\frac{\tilde{m}}{\mu}}\sqrt{1 + \left(\frac{\varpi_Y^2 - \varpi_X^2}{\omega_+^2 - \omega_-^2} \right)} \right)^2 \langle \eta_+^2 \rangle,$$

$$2\tilde{m}\langle R_{AC}^2 \rangle = \left(\sqrt{1 + \left(\frac{\varpi_Y^2 - \varpi_X^2}{\omega_+^2 - \omega_-^2} \right)} + \frac{\mu}{m_C}\sqrt{\frac{\tilde{m}}{\mu}}\sqrt{1 - \left(\frac{\varpi_Y^2 - \varpi_X^2}{\omega_+^2 - \omega_-^2} \right)} \right)^2 \langle \eta_-^2 \rangle$$

$$+ \left(\sqrt{1 - \left(\frac{\varpi_Y^2 - \varpi_X^2}{\omega_+^2 - \omega_-^2} \right)} + \frac{\mu}{m_C}\sqrt{\frac{\tilde{m}}{\mu}}\sqrt{1 + \left(\frac{\varpi_Y^2 - \varpi_X^2}{\omega_+^2 - \omega_-^2} \right)} \right)^2 \langle \eta_+^2 \rangle,$$

Neglecting terms in $\delta^2/(\varpi_Y^2 - \varpi_X^2)$, $\omega_-^2 \approx \varpi_X^2$ and $\omega_+^2 \approx \varpi_Y^2$. Thus

$$\langle R_{AB}^2 \rangle \approx \frac{1}{\tilde{m}} \langle \eta_-^2 \rangle + \frac{1}{\mu}\left(\frac{\mu}{m_B}\right)^2 \langle \eta_+^2 \rangle$$

$$= \frac{\hbar\omega_- \eta_-^{\text{eff}}}{\tilde{m}\omega_-^2} + \left(\frac{\mu}{m_B}\right)^2 \frac{\hbar\omega_+ \eta_+^{\text{eff}}}{\mu\omega_+^2}.$$

Similarly,

$$\langle R_{AC}^2 \rangle = \frac{\hbar\omega_- \eta_-^{\text{eff}}}{\tilde{m}\omega_-^2} + \left(\frac{\mu}{m_C}\right)^2 \frac{\hbar\omega_+ \eta_+^{\text{eff}}}{\mu\omega_+^2}.$$

More explicitly,

$$\langle R_{AH}^2 \rangle \approx \frac{\hbar\eta_-^{\text{eff}}}{\sqrt{2k\tilde{m}}} + \tfrac{4}{9}\frac{\hbar\eta_+^{\text{eff}}}{\sqrt{(k_{BC} + \frac{5}{9}k)\mu}} \cong \frac{\hbar\eta_-^{\text{eff}}}{\sqrt{6k\tilde{m}_H}} + \tfrac{4}{9}\sqrt{\tfrac{3}{2}}\frac{\hbar\eta_+^{\text{eff}}}{\sqrt{(k_{BC} + \frac{5}{9}k)m_H}},$$

$$\langle R_{AD} \rangle \approx \frac{\hbar\eta_-^{\text{eff}}}{\sqrt{2k\tilde{m}}} + \tfrac{1}{9}\frac{\hbar\eta_+^{\text{eff}}}{\sqrt{(k_{BC} + \frac{5}{9}k)\mu}} = \frac{\hbar\eta_-^{\text{eff}}}{\sqrt{6k\tilde{m}_H}} + \tfrac{1}{9}\sqrt{\tfrac{3}{2}}\frac{\hbar\eta_+^{\text{eff}}}{\sqrt{(k_{BC} + \frac{5}{9}k)m_H}}.$$

Thus, for any given *excess* energy $E - F(X_A)$ (i.e., η_I^{eff}), $\langle R_{AH}^2 \rangle$ will exceed $\langle R_{AD}^2 \rangle$.

The fact that $\langle R_{AH}^2 \rangle > \langle R_{AD}^2 \rangle$ implies that the AH bond is stretched more than AD bond at any excess energy. Alternatively one can conclude that less total energy is needed to "break" (i.e., to effect T–V transfer *and* extend to or beyond some critical distance) the AH bond, so the threshold for which *H departs* leaving AD^+ should be lower than that when D departs leaving MH^+. Indeed experimentally, AD^+ is observed to form at lower collision energies than AH^+.

4. Summary

We have introduced a model dynamics to use in treating the T–V energy transfer process that seems to be the rate-limiting step in the $M^+ + H_2 \rightarrow MH^+ + H$ reaction, with M = B, Al, Ga. In applying this model, we:

(1) Fit our fully *ab initio* $M^+ + H_2$ potential energy surfaces (with M = B, Al, Ga) to a two-dimensional model potential form.
(2) Show how to extract from local surface curvature information the range (a) and strength (v) parameters needed to use the model put forth here in a predictive manner.
(3) Used this model potential within a purely classical trajectory study to conclude that collisional-to-vibrational energy transfer thresholds seem to correlate reasonably well with experimental reaction thresholds for the $M^+ + H_2$, D_2, HD cases at hand.

However, this classical treatment of the model displayed significantly lower thresholds for $M^+ + D_2$ excitation than for $M^+ + H_2$, and it was not of adequate detail to treat the $M^+ + HD \rightarrow MH^+, MD^+$ threshold asymmetry. Therefore, we:
(4) Introduced a locally quadratic approximation to the potential surface to effect a quantal analysis of the T–V energy transfer process, which suggests facile transfer occurs in regions of the potential surface where certain resonance conditions are met.

(5) Introduced a coupled three-atom classical dynamics model to examine internal mean square displacements in these energized M^+HD transient species formed via T–*V* energy transfer,that allowed us to suggest (i) why MD^+ is formed at considerably lower collision energies than MH^+ in the $M^+ + HD$ reactions, and (ii) why the $M^+ + H_2$ and $M^+ + D_2$ *reaction* thresholds are very similar although the M^+D_2 *T–V* excitation thresholds are lower than those for M^+H_2.
(6) Showed that the probability of *T–V* transfer varies as $\hbar\Gamma^2K^2/\omega_Y$ $(=\hbar b^2/\sqrt{\tilde{m}k_{BC}})$, which is a small number, in agreement with the small cross-sections seen experimentally.

In future applications, we foresee our model dynamics being used in either of two modes:

1. From locally computed potential surface information (which is assumed to be repulsive along one coordinate x, and reasonably harmonic along another y), the strength v and range (a or Γ) parameters are extracted. Threshold energies can then be predicted, $F(X_A) = e^z F_0 = e^z\omega_X^2/\Gamma^2 = 0.722\omega_Y^2\tilde{m}/a^2$, in terms of the frequency of the BC mode to be excited, the mass $\tilde{m}$, and the repulsive range parameter a.
2. Alternatively, given experimental knowledge of (*T–V* rate limited) reaction threshold energies $F(X_A)$, one can estimate the repulsive range parameter $a = (e^z(1.53)^2\omega_Y^2\tilde{m}/F(X_A))^{1/2}$ for various isotopic B–C species (for which $\tilde{m}$, ω_Y, and $F(X_A)$ vary). The same range parameter a should be determined for all isotopes.

Acknowledgements. This work was supported by the Office of Naval Research and by the National Science Foundation grant number CHE9116286. One of us (MRC-T), would like to thank Dr. Jeff Nichols and Mr. Mark Robertson for valuable discussions.

References

1. Armentrout PB (1990) Int Rev Phys Chem 9:115; Elkind JL, Armentrout PB, unpublished results
2. Henglein A (1966) In: Ausloos PJ (ed) Ion–Molecule reactions in the gas phase, American Chemical Society, Washington, p 63; Mahan BH (1970) J Chem Phys 52:5221; Rapp D, Kassal T (1969) Chem Rev 69:61; Rapp Ds (1971) Quantum mechanics, Chapter 24. Holt, New York.
3. Gutowski M, Robertson M, Rusho J, Nichols J, Simons J (1993) J Chem Phys 99:2601
4. Press WH, Teukolsky SA, Vetterling WT, Flannery BP (1986) Numerical recipes in Fortran, Ind Ed. Cambridge University Press, New York, p 708
5. Raff LM, Thompson DL (1985) In: Baer M (ed) Theory of chemical reaction dynamics, Vol III. CRC Press, Boca Raton, FL, p 13
6. Lambert JD (1977) Vibrational and rotational relaxation in gases. Clarendon Press, Oxford, p 43
7. Merzbacher E, Quantum mechanics, 2nd ed. Wiley, New York.
8. For impulsive collisions such as those thought to be operative here, this assumption can be questioned. However, we note that equal distribution of excess energy among modes is not required of *all* collisions to render this assumption appropriate. In particular, it need not be stated in terms of adequate *time* for energy randomization, but can be viewed as the ensemble of collisions that produce reaction possessing essentially equal excess energy content for the two modes.
9. Such approximations to phase–space distribution functions have been shown (Bowman JM, Kuppermann A, Schatz GC (1973) Chem Phys Lett 19:20 to produce incorrect cross-sections when compared to proper quantum predictions. However, they were seen to be qualitatively correct especially near thresholds, which is our main focus here.